


Article

# Origin of the Low Magnetic Moment in Fe<sub>2</sub>AlTi: An Ab Initio Study

Martin Friák<sup>1,\*</sup>, Anton Slávik<sup>1,2</sup>, Ivana Miháliková<sup>1,2</sup>, David Holec<sup>3</sup> , Monika Všianská<sup>4,1,5</sup>, Mojmír Šob<sup>4,1,5</sup>, Martin Palm<sup>6</sup> and Jörg Neugebauer<sup>6</sup>

<sup>1</sup> Institute of Physics of Materials, Academy of Sciences of the Czech Republic, Žitkova 22, CZ-616 62 Brno, Czech Republic; tono.slavik@gmail.com (A.S.); ivanamihalik2@gmail.com (I.M.); Monika.Vsianska@seznam.cz (M.V.); mojmir@ipm.cz (M.Š.)

<sup>2</sup> Department of Condensed Matter Physics, Faculty of Science, Masaryk University, Kotlářská 2, CZ-611 37 Brno, Czech Republic

<sup>3</sup> Department of Physical Metallurgy and Materials Testing, Montanuniversität Leoben, Franz-Josef-Strasse 18, A-8700 Leoben, Austria; david.holec@unileoben.ac.at

<sup>4</sup> Central European Institute of Technology, CEITEC MU, Masaryk University, Kamenice 5, CZ-625 00 Brno, Czech Republic

<sup>5</sup> Department of Chemistry, Faculty of Science, Masaryk University, Kotlářská 2, CZ-611 37 Brno, Czech Republic

<sup>6</sup> Max-Planck-Institut für Eisenforschung GmbH, Max-Planck-Str. 1, D-40237 Düsseldorf, Germany; m.palm@mpie.de (M.P.); neugebauer@mpie.de (J.N.)

\* Correspondence: friak@ipm.cz

Received: 1 September 2018; Accepted: 12 September 2018; Published: 14 September 2018



**Abstract:** The intermetallic compound Fe<sub>2</sub>AlTi (alternatively Fe<sub>2</sub>TiAl) is an important phase in the ternary Fe-Al-Ti phase diagram. Previous theoretical studies showed a large discrepancy of approximately an order of magnitude between the ab initio computed magnetic moments and the experimentally measured ones. To unravel the source of this discrepancy, we analyze how various mechanisms present in realistic materials such as residual strain effects or deviations from stoichiometry affect magnetism. Since in spin-unconstrained calculations the system always evolves to the spin configuration which represents a local or global minimum in the total energy surface, finite temperature spin effects are not well described. We therefore turn the investigation around and use constrained spin calculations, fixing the global magnetic moment. This approach provides direct insight into local and global energy minima (reflecting metastable and stable spin phases) as well as the curvature of the energy surface, which correlates with the magnetic entropy and thus the magnetic configuration space accessible at finite temperatures. Based on this approach, we show that deviations from stoichiometry have a huge impact on the local magnetic moment and can explain the experimentally observed low magnetic moments.

**Keywords:** Fe<sub>2</sub>AlTi; Fe<sub>2</sub>TiAl; Heusler; magnetism; ab initio; stability; off-stoichiometry; strain

## 1. Introduction

The Fe-Al-Ti ternary system is the basis for materials with a wide range of technologically interesting properties. Notable are, for example, medical applications [1,2], their ability to form oxygen-containing inclusions strengthening steels [3], their potential for high-temperature applications [4–9], and more [10–16]. For a detailed overview, see the review by Palm and Lacaze in Ref. [17]. A subset of these high-temperature materials are two-phase Fe-Al-Ti superalloys (e.g., [18–21]) containing an off-stoichiometric Fe<sub>2</sub>AlTi intermetallic compound.

Stoichiometric Fe<sub>2</sub>AlTi crystallizes in the Heusler L<sub>21</sub>-structure. It was included in an extensive theoretical study by Gilleßen and Dronskowski in which they calculated properties of 810 different

compounds with either Heusler [22] or inverse Heusler [23] structure type. Elastic properties of Fe<sub>2</sub>AlTi were recently theoretically studied at ambient conditions [24] as well as under hydrostatic pressures [25]. The thermal expansion coefficient, Debye temperature, and heat capacity at temperatures up to 1200 K and pressures up to 250 GPa were determined [25]. The electronic structure of Fe<sub>2</sub>AlTi was experimentally analyzed by Kourov et al. [26], and it was found strongly spin-polarized in agreement with theoretical studies (see, e.g., Shreder et al. [27]).

There is a long-lasting discrepancy between the experimental magnetic moment of Fe<sub>2</sub>AlTi and the theoretical prediction of this quantity, which is nearly an order of magnitude higher. In particular, experimental values of 0.1  $\mu_B$  per formula unit (abbreviated as f.u.) reported in Ref. [28] or 0.11  $\mu_B$ /f.u. in Ref. [29] for  $T = 4.2$  K, are significantly lower than the results of density functional theory (DFT) calculations (e.g., 0.9  $\mu_B$ /f.u. in Refs. [27,30]). This is indeed very interesting because it is well-known that DFT calculations mostly predict the magnetic moment of materials very well. For example, that of Fe is predicted to be 2.25  $\mu_B$  [31], matching perfectly the experimental value of 2.22  $\mu_B$  [32].

To resolve this issue, we studied in detail how deviations from perfect crystal (e.g., deviations in stoichiometry, internal strain, etc.) affect the local moment. Considering that in typical spin-unconstrained calculations the system always evolves to the spin configuration which represents a local or global minimum at the total energy surface, we turn the investigation around and use constrained spin calculations. Fixing the global magnetic moment to a set of different values, we obtain direct insight into local and global energy minima (reflecting metastable and stable spin phases). Employing these fixed-spin moment (FSM) quantum-mechanical calculations, we determine thermodynamic, electronic, and structural properties of both stoichiometric and off-stoichiometric Fe<sub>2</sub>AlTi at different magnetic states. Based on these calculations, we explain the discrepancy discussed above.

## 2. Materials and Methods

The calculations were performed within the framework of density functional theory [33,34] using the Vienna Ab initio Simulation Package (VASP) [35,36] and projector augmented wave pseudopotentials [37,38]. The exchange and correlation energy was treated in the generalized gradient approximation (GGA) as parametrized by Perdew and Wang [39] using the Vosko–Wilk–Nusair correction [40]. We used a plane-wave energy cut-off of 350 eV with a  $10 \times 10 \times 10$  Monkhorst-Pack k-point mesh. The system is described with the help of a cube-shaped 16-atom supercell containing four formula units of Fe<sub>2</sub>AlTi (see both the stoichiometric case in Figure 1a and supercells with anti-sites in Figures 1b,c).

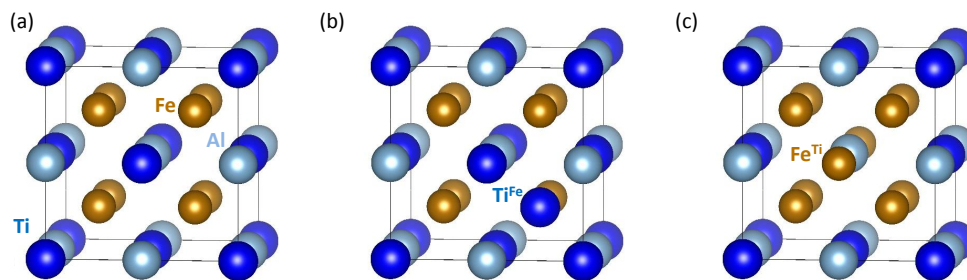


**Figure 1.** (a) Schematic visualization of the cube-shaped 16-atom Fe<sub>2</sub>AlTi supercell used in our calculations. Two types of substituted states (discussed below) when either (b) Ti replaces Fe or (c) Fe replaces Ti.

The FSM approach [31,41–47] allows the total magnetic moment of a computational supercell to be fixed at a specific value. The local magnetic moments are free to change (given the overall global constraint) regarding their magnitudes as well as their orientations (here only parallel or anti-parallel).

When fixing the total magnetic moment of the computational cell, all local magnetic moments are initially oriented in a parallel manner (a ferromagnetic state).

### 3. Results

In order to identify the reason why the DFT computed ground state of  $\text{Fe}_2\text{AlTi}$  shows a much higher magnetic moment than is observed experimentally, we systematically searched for additional minima on the total energy landscape. These minima correspond to metastable phases and may correspond to magnetic states that are closer to the experimental one. We therefore calculated the properties of different magnetic states of stoichiometric  $\text{Fe}_2\text{AlTi}$  as a function of fixed-spin moment. Figure 2 summarizes the computed energies, lattice parameters, and local magnetic moments of Fe and Ti atoms as functions of the fixed-spin moment. As visualized in Figure 2a, there was only a single minimum. The lowest energy was predicted for a state with the FSM of  $0.925 \mu_B$  per formula unit. The local magnetic moments of the Fe and Ti atoms were  $0.610$  and  $-0.279 \mu_B/\text{atom}$ , respectively (the negative sign indicates an anti-parallel orientation—i.e.,  $\text{Fe}_2\text{AlTi}$  is in a ferrimagnetic state, in contrast to the initial ferromagnetic state of our calculations when all magnetic moments were parallel). The opposite orientation of the local magnetic moment of Ti lowered the energy of the systems and resulted from a full relaxation of all degrees of freedom in our calculations. Our predicted values agreed with those previously reported in Ref. [48] ( $0.95 \mu_B/\text{f.u.}$ ,  $0.67$  and  $-0.28 \mu_B/\text{atom}$ ).

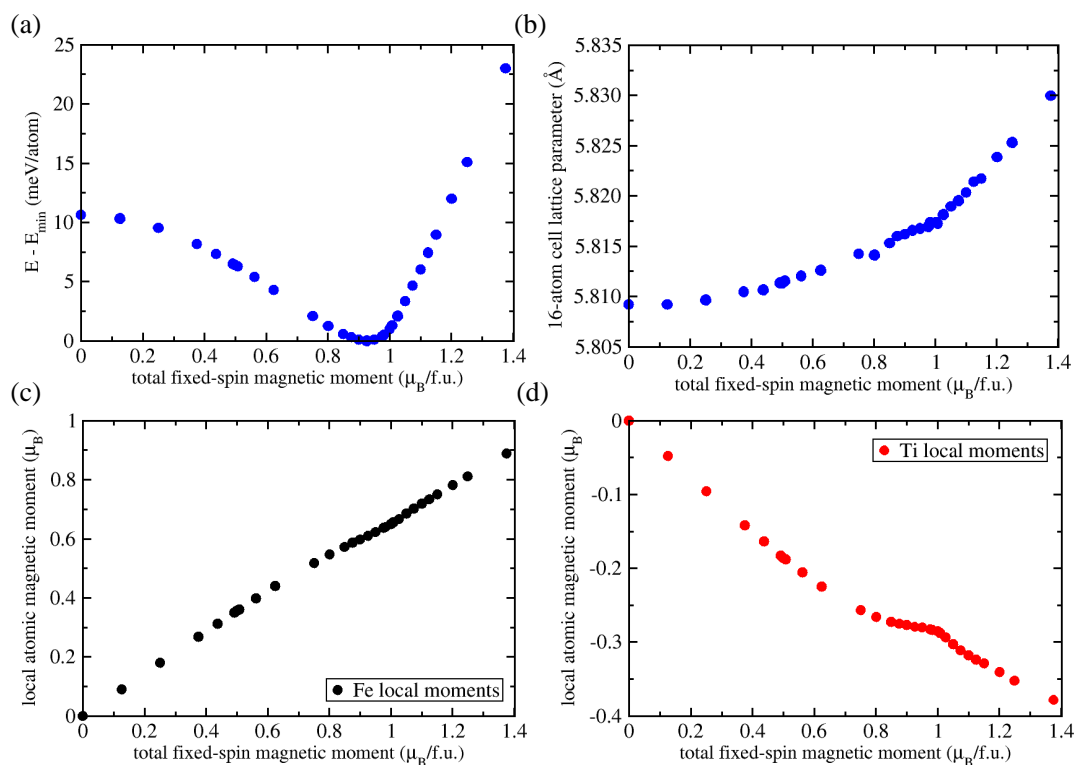


**Figure 2.** Computed dependencies of (a) the total energy (referenced to the lowest obtained energy), (b) a 16-atom supercell lattice parameter and local magnetic moments of (c) Fe and (d) Ti atoms as functions of the fixed-spin value of the total magnetic moment per formula unit.

Figure 2b shows that the lattice parameter of our cube-shaped 16-atom supercell monotonously increased with increasing fixed-spin moment (except for some small scatter in our data points). The lowest energy state was predicted to have a lattice parameter of  $5.817 \text{ \AA}$ , in agreement with  $5.879 \text{ \AA}$  calculated by Fecher et al. [48]. They also agreed with the experimental values of  $5.879 \text{ \AA}$  reported by Buschow and van Engen [29], as well as  $5.858 \text{ \AA}$  published in Ref. [27] and  $5.878 \text{ \AA}$  found in Ref. [19].

Parts (c) and (d) of Figure 2 depict local magnetic moments of Fe and Ti atoms. The opposite sign of the Fe in Figure 2c and Ti Figure 2d moments implies an anti-parallel orientation. The absolute value of the local magnetic moments of the Fe and Ti atoms increased with increasing FSM value.

Our calculations revealed an interesting feature of the states around the lowest-energy state (see Figure 2d). The local magnetic moments at Ti atoms decreased less steeply just prior to reaching the state with the lowest energy and started to decrease more steeply again only when reaching states with FSM higher than about  $1 \mu_B$  per formula unit. In contrast, for these values of the FSM, the local magnetic moments of the Fe atoms showed a significantly smaller deviation from a monotonously increasing trend (see Figure 2c). Aluminium atoms (not shown) were predicted to have negligible local magnetic moments (lower than  $0.02 \mu_B/\text{atom}$ ), and were therefore considered in the following discussion as non-magnetic.

We thus conclude that in the case of strain-free stoichiometric  $\text{Fe}_2\text{AlTi}$ , only a single energy minimum exists (i.e., metastable configurations with a low spin state do not exist). We now explore alternative mechanisms that may explain the discrepancy between theoretical and experimental data. First, our fixed-spin-moment analysis showed that the non-magnetic state was higher in energy than the lowest-energy magnetic state. However, this difference was only  $10.6 \text{ meV/atom}$  (see Figure 2a). In fact, its energy was so close to the lowest-energy ferrimagnetic state that it may be thermodynamically stabilized in  $\text{Fe}_2\text{AlTi}$  samples already at rather low temperatures. As we have only  $T = 0 \text{ K}$  results, we used Boltzmann statistics to consider approximatively, for example, a temperature of  $100 \text{ K}$  which was chosen because it is rather close to the magnetic transition temperature of  $123 \text{ K}$  detected by Buschow and van Engen [29]. The probability of finding the measured samples in a non-magnetic state, instead in the ferrimagnetic lowest-energy one, was significant even at this low temperature (22.6%). Such non-magnetic fluctuations could be easily accommodated by the surrounding ferrimagnetic matrix: the non-magnetic state had a lattice parameter ( $5.809 \text{ \AA}$ ) very similar to that of the lowest energy ferrimagnetic state ( $5.817 \text{ \AA}$ ) as seen in Figure 2b. Importantly, while the overall magnetization can be reduced due to statistically quite high probability of non-magnetic states, this probability became significant only at temperatures of at least  $30\text{--}40 \text{ K}$ . On the other hand, the measurements by Buschow and van Engen [29] were performed at  $4.2 \text{ K}$ . We can therefore also exclude this mechanism as the origin of the low magnetic moment.

Next, we simulated the impact that local strain and deformations may have on the local magnetic moments. We therefore simulated two types of cell-shape deformations. For small strains, these deformations are associated with the cubic-symmetry elastic constants  $C_{44}$  and  $C'$ . A trigonal deformation with strain  $\varepsilon$  modifies the original set of cubic-cell vectors  $[1, 0, 0]$ ,  $[0, 1, 0]$ , and  $[0, 0, 1]$  to a new one  $[1, \varepsilon, \varepsilon]$ ,  $[\varepsilon, 1, \varepsilon]$  and  $[\varepsilon, \varepsilon, 1]$ , tetragonal deformation leads to unit-cell vectors  $[1-\varepsilon/2, 0, 0]$ ,  $[0, 1-\varepsilon/2, 0]$ , and  $[0, 0, 1+\varepsilon]$ . Regarding the terminology, positive strains (e.g., trigonal ones) are tensile along the  $[111]$  direction while compressing the crystal within the perpendicular plane. Below, such strains are called tensile. Figure 3 summarizes our results related to trigonally deformed  $\text{Fe}_2\text{AlTi}$  for different values of FSM and selected values of strain  $\varepsilon$ .

As shown in Figure 3a, starting at a strain  $\varepsilon = -0.06$  an energy minimum at non-zero FSM was observed. This minimum is related to a ferrimagnetic state. Going to the strain  $\varepsilon = -0.07$ , the energy minimum corresponds to a non-magnetic state with  $\text{FSM} = 0$  (see Figure 3b). This behavior was confirmed for strains  $\varepsilon = -0.075$  and  $-0.080$  (not shown). The ferrimagnetic states for positive (tensile) strains (along the  $[111]$  direction) had lower magnetic moments compared to the strain-free states (see Figure 3c,d). However, the reduction was much smaller than in the case of negative strains.  $\text{Fe}_2\text{AlTi}$  thus exhibited a strong asymmetry between tensile and compressive loading. Importantly, negative strains from  $-0.07$  onwards destabilized the ferrimagnetic state in favor of the non-magnetic one.

It is tempting to assign the zero/vanishingly low magnetic moment to the experimentally observed low moment. Unfortunately, this mechanism became active only at large strains beyond  $-0.07$ . Such large compressive strains (along the  $[111]$  direction) can only appear locally (e.g., at grain

boundaries, close to dislocation cores or other point or extended defects). In a typical experimental sample, the concentration of these extended defects is too low to explain the experimentally observed low magnetic moment. We applied the same approach to tetragonal deformations. However, the local moments were stable for strains up to  $\pm 0.080$  (not shown). We can therefore also exclude strains as a possible source of low magnetic moments.

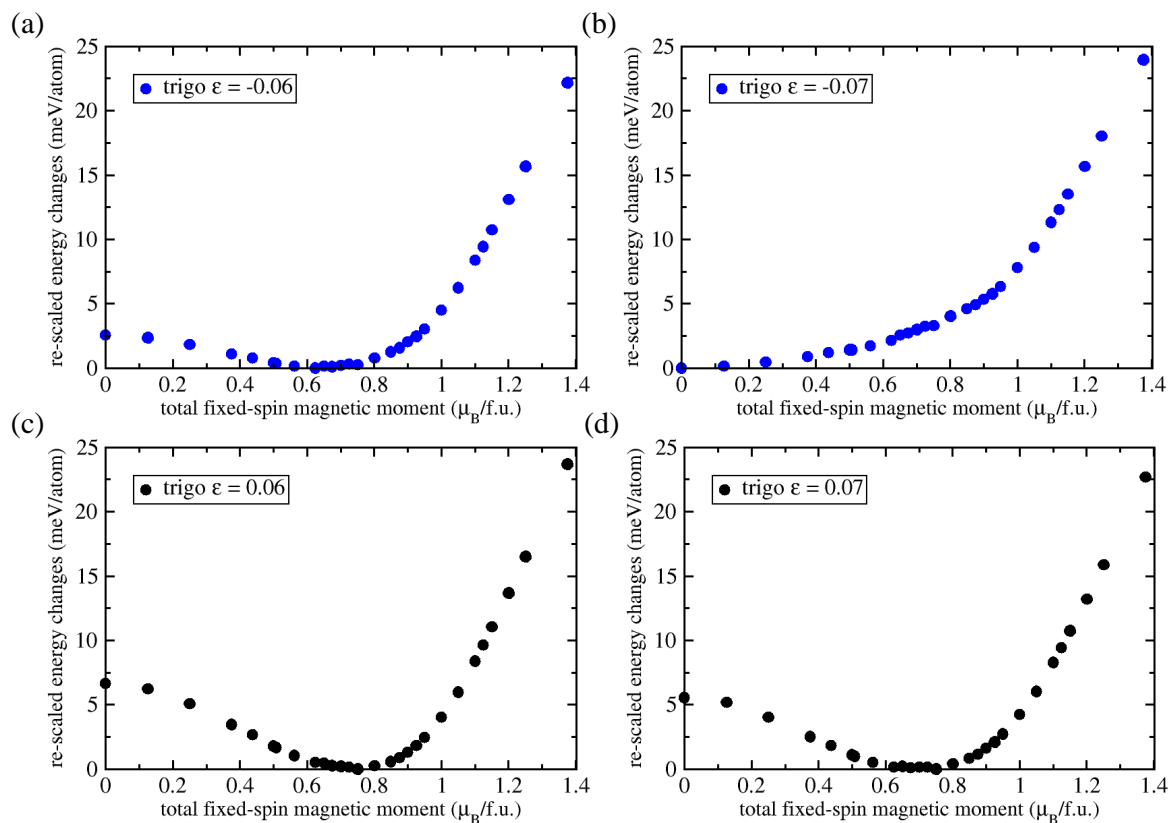


**Figure 3.** Ab initio calculated energies of trigonally deformed  $\text{Fe}_2\text{AlTi}$  for different values of fixed-spin moment (FSM). Results are shown for selected values of strain  $\epsilon$  including negative (a)  $-0.06$  and (b)  $-0.07$  and positive (c)  $0.06$  and (d)  $0.07$ . The energies for each value of  $\epsilon$  and different values of FSM are shown as differences with respect to the lowest energy for a given value of  $\epsilon$ .

As a further mechanism we studied deviations from ideal stoichiometry. Experimentally, it is highly non-trivial to synthesize truly stoichiometric single-phase  $\text{Fe}_2\text{AlTi}$  samples. The reason is that during cooling from the melt Laves phases, such as  $\text{Fe}_2\text{Ti}$ , form [49,50]. These phases only slowly dissolve when approaching lower temperatures due to sluggish kinetics. Consequently, most  $\text{Fe}_2\text{AlTi}$  samples are actually off-stoichiometric. We simulated this situation by introducing off-stoichiometric defects such as  $\text{Fe}^{\text{Ti}}$  or  $\text{Ti}^{\text{Fe}}$  anti-sites. The calculations were performed with the help of our computational 16-atom supercell. The anti-sites are marked as  $\text{Ti}^{\text{Fe}}$  in Figure 1b and  $\text{Fe}^{\text{Ti}}$  in Figure 1c, respectively. Our results are depicted in Figure 4. To allow for a direct comparison with the stoichiometric results, the trends are displayed using the same formula unit consisting of four atoms as a reference.

Going to an excess Fe concentration  $\text{Fe}_9\text{Al}_4\text{Ti}_3$  (56.25 at. % Fe and only 18.75 at. % Ti), we found two energy minima (see Figure 4a). The lowest energy was found for a state with fixed-spin moment equal to  $0.1 \mu_B$ . This state was separated by an energy barrier of 17.7 meV/atom. The higher-lying energy minimum (higher by 3.7 meV/atom) corresponded to a state with the FSM of  $0.938 \mu_B$  per four atoms. The presence of two states is related to the presence of two inequivalent types of Fe atoms

which exhibit different magnetic states. The off-stoichiometric anti-site Fe atom was in a high-spin state. Its local magnetic moment was  $2.55 \mu_B$ . Due to the presence of the  $\text{Fe}^{\text{Ti}}$  anti-site, the surrounding eight Fe atoms had their local magnetic moment reduced to  $0.29 \mu_B$  (see the inset in Figure 4a).

In the lowest energy state, the magnetic moment of the excess Fe atom was anti-parallel to those of regular Fe atoms. The Ti atoms showed a qualitatively similar behavior (their magnetic moments were anti-parallel to those of regular Fe atoms). The lattice parameter decreased for increasing FSM up to the value of  $\text{FSM} = 0.75 \mu_B$  (see Figure 4c). This magneto-volumetric behavior is very different from that of stoichiometric  $\text{Fe}_2\text{AlTi}$  (see Figure 2b).

We now study the opposite type of off-stoichiometry (i.e. Ti excess), creating a  $\text{Ti}^{\text{Fe}}$  anti-site defect in the 16-atom supercell (see Figure 4b). The single minimum at  $0.175 \mu_B$  at the energy surface was extremely shallow—only  $0.05 \text{ meV/atom}$  lower than the non-magnetic state at zero FSM. Due to the low energy difference, even low temperatures were sufficient to stabilize non-magnetic configurations. Thus, this type of substitution will also lead to states with very low magnetic moments.

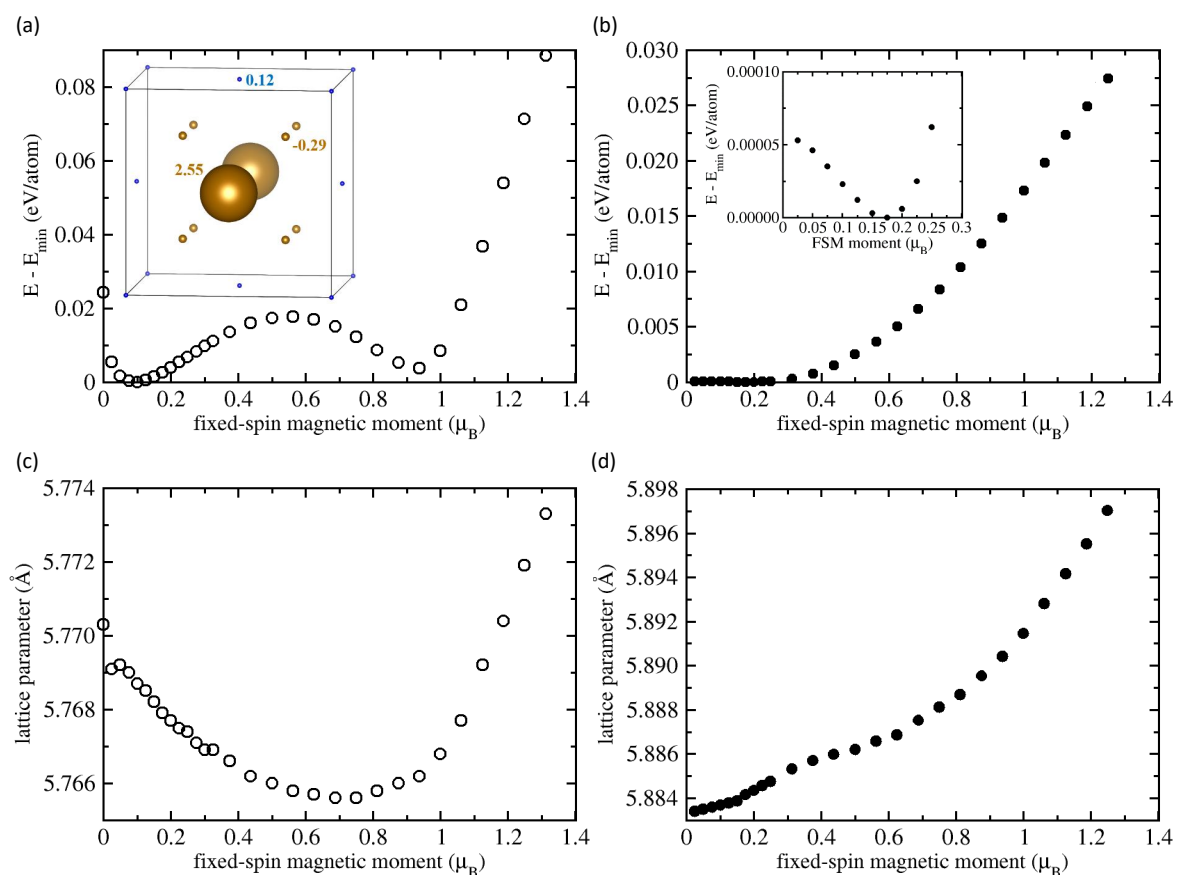


**Figure 4.** Computed total energies for non-stoichiometric  $\text{Fe}_2\text{AlTi}$ . The results for the excess Fe concentration  $\text{Fe}_{56.25}\text{Al}_{25}\text{Ti}_{18.75}$  are shown in (a,c). For excess Ti, the corresponding results are displayed in (b,d). The values of the FSM are per four atoms in order to allow for a comparison with the figures visualizing results for the stoichiometric  $\text{Fe}_2\text{AlTi}$  discussed above. The inset within part (a) shows the local magnetic moments of atoms in the state with the lowest energy (some atoms are shown with their periodic images) and that in part (b) magnifies an extremely shallow energy minimum.

#### 4. Discussion

The above results clearly indicate that off-stoichiometry is the most likely candidate to resolve the large discrepancy between measured and computed magnetic moments. Inspecting the ternary Fe-Al-Ti phase diagram at temperatures of 800, 900 and 1000 °C (e.g., Ref. [17]), the experimentally

determined region of existence of  $\text{Fe}_2\text{AlTi}$  does not contain stoichiometric  $\text{Fe}_2\text{AlTi}$ . Rather, it contains only Fe-rich (Ti-lean) off-stoichiometric  $\text{Fe}_2\text{AlTi}$  phases with a very wide range of excess Fe (even over 25 at. %). Thus, off-stoichiometric regions are very probably present in experimental samples. As discussed in the previous section, off-stoichiometry is realized by anti-site defects. Since these defects are anti-ferromagnetically coupled to the surrounding Fe atoms, such defects reduce the net magnetic moment of the sample. For the concentration of Fe anti-sites considered here (6.25 at. % excess Fe, see Figure 4a), this lowest-energy state has the magnetic moment of  $0.1 \mu_B$  per 4 atoms, which is practically identical to the experimental magnetic moments ( $0.1 \mu_B$  per formula unit reported in Ref. [28] or  $0.11 \mu_B/\text{f.u.}$  in Ref. [29]).

Our conclusion also fits with the interpretation given by Buschow and van Engen [29]. They critically assessed their measured values of the saturation magnetization and the transition temperature. One critical issue they identified was that the value of the magnetic moment in  $\text{Fe}_2\text{TiAl}$  is too low for a (relatively high) transition temperature of 123 K. To resolve this issue, they suggested that the  $\text{Fe}_2\text{AlTi}$  compound is either Pauli paramagnetic or antiferromagnetic. Our findings, when the anti-site Fe atoms in the Fe-rich off-stoichiometric case have their local magnetic moment anti-parallel to Fe atoms on the regular Fe sublattice, agree with the antiferromagnetic hypothesis of Buschow and van Engen.

## 5. Conclusions

Using DFT fixed-spin-moment calculations we systematically analyzed the thermodynamic stability, structure, and magnetic properties of different magnetic states of stoichiometric and off-stoichiometric  $\text{Fe}_2\text{AlTi}$ . Based on these results we could systematically test various mechanisms that could explain the exceptionally low magnetic moment measured for  $\text{Fe}_2\text{AlTi}$ . For the stoichiometric case, none of the mechanisms studied (i.e., trigonal and tetragonal strains, finite-temperature spin excitations) could account for this effect. Considering Fe-rich and Ti-rich off-stoichiometric configurations with an excess of 6.25 at. % of Fe or Ti atoms, the net magnetization drops to very low values. In the case of  $\text{Fe}_2\text{AlTi}$ , off-stoichiometric alloys with excess Fe are more relevant because the experimental Fe-Al-Ti phase diagram contains only Fe-rich phases above  $800^\circ\text{C}$ . For the Fe-rich alloy, the energetically preferred state has a net magnetic moment close to the measured one. Our study shows how sensitively magnetism is affected by off-stoichiometries in the alloy composition. Even relatively small changes of a few percent can cause changes of an order of magnitude in magnetic moments. Therefore, a mandatory requirement when comparing ab initio computed moments with experimental values is to critically assess the stoichiometry of the experimental samples.

**Author Contributions:** Conceptualization, M.F.; Methodology, D.H.; Validation, A.S. and I.M., Thermodynamic Analysis, M.P.; Resources, M.Š. and J.N.; Writing—Original Draft Preparation, M.F.; Writing—Review & Editing, A.S., I.M., D.H., M.P., M.V., J.N. and M.Š.; Visualization, M.F. and M.V.; Supervision, M.Š., M.P., J.N. and M.F.; Project Administration, M.F.; Funding Acquisition, M.F.

**Funding:** The authors acknowledge the Czech Science Foundation for the financial support received under the Project No. 17-22139S (M.F., A.S., I.M.). Additional resources were provided by the Academy of Sciences of the Czech Republic through the Fellowship of J. E. Purkyně (M.F.) and by the Ministry of Education, Youth and Sports of the Czech Republic under the Project CEITEC 2020, LQ1601 (M.Š., M.V.).

**Acknowledgments:** M.F., A.S., I.M., M.V. and M.Š. also acknowledge supports from the Academy of Sciences of the Czech Republic (Institutional Project No. RVO:68081723) and from the Ministry of Education, Youth and Sports of the Czech Republic via the research infrastructure IPMINFRA, LM2015069. Computational resources were made available by the Ministry of Education, Youth and Sports of the Czech Republic under the Projects CESNET (Project No. LM2015042), CERIT-Scientific Cloud (Project No. LM2015085) and IT4Innovations National Supercomputer Center (Project No. LM2015070) within the program Projects of Large Research, Development and Innovations Infrastructures. Figure 1 and subset in Figure 4a were visualized using the VESTA package [51–53]. We also acknowledge very fruitful discussions with Yvonna Jirásková from IPM in Brno.

**Conflicts of Interest:** The authors declare no conflict of interest.

## References

1. Zwicker, U.; Breme, J.; Nigge, K. *Mikrochim. Acta Suppl.* **1985**, *11*, 333.
2. Zwicker, U. Investigations on the TiAl<sub>5</sub>Fe<sub>2.5</sub> alloy as implant material. *Z. Metallkd.* **1986**, *77*, 714–720.
3. Jung, I.H.; Decterov, S.A.; Pelton, A.D. Computer applications of thermodynamic databases to inclusion engineering. *ISIJ Int.* **2004**, *44*, 527–536. [[CrossRef](#)]
4. Gorzel, A.; Palm, M.; Sauthoff, G. Constitution-based alloy selection for the screening of intermetallic Ti-Al-Fe alloys. *Z. Metallkd.* **1999**, *90*, 64–70.
5. Palm, M. Concepts derived from phase diagram studies for the strengthening of Fe-Al-based alloys. *Intermetallics* **2005**, *13*, 1286–1295. [[CrossRef](#)]
6. Brady, M.P.; Smialek, J.L.; Brindley, W.J. Oxidation-Resistant Ti-Al-Fe Alloy for Diffusion Barrier Coatings. US Patent No. 5,776,617, 7 July 1998.
7. Dew-Hughes, D.; Kaufman, L. Ternary phase diagrams of the manganese-titanium-iron and the aluminum-titanium-iron systems: A comparison of computer calculations with experiment. *Calphad* **1979**, *3*, 175–203. [[CrossRef](#)]
8. Raghavan, V. Al-Fe-Ti (aluminum-iron-titanium). *J. Phase Equilib.* **1993**, *14*, 618–619. [[CrossRef](#)]
9. Raghavan, V. Al-Fe-Ti (Aluminum-Iron-Titanium). *J. Phase Equilib.* **2002**, *23*, 367–374. [[CrossRef](#)]
10. Krein, R.; Palm, M.; Heilmaier, M. Characterization of microstructures, mechanical properties, and oxidation behavior of coherent A2+L2<sub>1</sub> Fe-Al-Ti. *J. Mater. Res.* **2009**, *24*, 3412–3421. [[CrossRef](#)]
11. Capdevila, C.; Aranda, M.M.; Rementeria, R.; Chao, J.; Urones-Garrote, E.; Aldazabal, J.; Miller, M.K. Strengthening by intermetallic nanoprecipitation in Fe-Cr-Al-Ti alloy. *Acta Mater.* **2016**, *107*, 27–37. [[CrossRef](#)]
12. Nakata, J.; Terada, Y.; Takizawa, S.; Ohkubo, K.; Mohri, T.; Suzuki, T. Thermal conductivity in X<sub>2</sub>YZ heusler type intermetallic compounds. *Mater. Trans. JIM* **1996**, *37*, 442–447. [[CrossRef](#)]
13. Kainuma, R.; Urushiyama, K.; Ishikawa, K.; Jia, C.; Ohnuma, I.; Ishida, K. Ordering and phase separation in bcc aluminides of the Ni-Fe-Al-Ti system. *Mater. Sci. Eng. A* **1997**, *240*, 235–244. [[CrossRef](#)]
14. Fomina, K.A.; Marchenkov, V.V.; Shreder, E.I.; Weber, H.W. Electrical and optical properties of X<sub>2</sub>YZ (X = Co, Fe; Y = Cr, Mn, Ti; Z = Ga, Al, Si) Heusler alloys. In *Solid State Phenomena; Trends in Magnetism*; Ustinov, V., Ed.; Russian Academy of Sciences, Institute for Metal Physics: Saint Petersburg, Russia, 2011; Volume 168–169, pp. 545. [[CrossRef](#)]
15. Brzakalik, K. Nearest-neighbor configurations of Fe atoms in Fe<sub>3-x</sub>Ti<sub>x</sub>Al ordered alloys. *Intermetallics* **2008**, *16*, 1053–1060. [[CrossRef](#)]
16. Suzuki, R.; Kyono, T. Thermoelectric properties of Fe<sub>2</sub>TiAl heusler alloys. *J. Alloys Compd.* **2004**, *377*, 38–42. [[CrossRef](#)]
17. Palm, M.; Lacaze, J. Assessment of the Al-Fe-Ti system. *Intermetallics* **2006**, *14*, 1291–1303. [[CrossRef](#)]
18. Krein, R.; Friak, M.; Neugebauer, J.; Palm, M.; Heilmaier, M. L<sub>21</sub>-ordered Fe-Al-Ti alloys. *Intermetallics* **2010**, *18*, 1360–1364. [[CrossRef](#)]
19. Palm, M.; Inden, G.; Thomas, N. The Fe-Al-Ti system. *J. Phase Equilib.* **1995**, *16*, 209–222. [[CrossRef](#)]
20. Palm, M.; Sauthoff, G. Deformation behaviour and oxidation resistance of single-phase and two-phase L<sub>21</sub>-ordered Fe-Al-Ti alloys. *Intermetallics* **2004**, *12*, 1345–1359. [[CrossRef](#)]
21. Michalcova, A.; Sencekova, L.; Rolink, G.; Weisheit, A.; Pesicka, J.; Stobik, M.; Palm, M. Laser additive manufacturing of iron aluminides strengthened by ordering, borides or coherent Heusler phase. *Mater. Des.* **2017**, *116*, 481–494. [[CrossRef](#)]
22. Gilleßen, M.; Dronskowski, R. A combinatorial study of full Heusler alloys by first-principles computational methods. *J. Comput. Chem* **2009**, *30*, 1290–1299. [[CrossRef](#)] [[PubMed](#)]
23. Gilleßen, M.; Dronskowski, R. A combinatorial study of inverse Heusler alloys by first-principles computational methods. *J. Comput. Chem* **2010**, *31*, 612–619. [[CrossRef](#)] [[PubMed](#)]
24. Adebambo, P.O.; Adetunji, B.I.; Olowofela, J.A.; Oguntuase, J.A.; Adebayo, G.A. Prediction of metallic and half-metallic structure and elastic properties of Fe<sub>2</sub>Ti<sub>1-x</sub>Mn<sub>x</sub>Al Heusler alloys. *Phys. B Condens. Matter* **2016**, *485*, 103–109. [[CrossRef](#)]
25. Xian-Kun, L.; Cong, L.; Zhou, Z.; Xiao-Hua, L. First-principles investigation on the structural and elastic properties of cubic-Fe<sub>2</sub>TiAl under high pressures. *Chin. Phys. B* **2013**, *22*.



26. Kourov, N.I.; Marchenkov, V.V.; Belozerova, K.A.; Weber, H.W. Specific Features of the Electrical Resistivity of Half-Metallic Ferromagnets Fe<sub>2</sub>MeAl (Me = Ti, V, Cr, Mn, Fe, Ni). *J. Exp. Theor. Phys.* **2014**, *118*, 426–431. [[CrossRef](#)]
27. Shreder, E.; Streltsov, S.V.; Svyazhin, A.; Lukoyanov, A.; Anisimov, V. Electronic structure and physical properties of Fe<sub>2</sub>MAI (M = Ti, V, Cr) Heusler alloys. In Proceedings of the Third International Symposium on Magnetism, Moscow, Russia, 26–30 June 2005.
28. Shreder, E.; Streltsov, S.V.; Svyazhin, A.; Makhnev, A.; Marchenkov, V.V.; Lukoyanov, A.; Weber, H.W. Evolution of the electronic structure and physical properties of Fe(2)MeAl (Me = Ti, V, Cr) Heusler alloys. *J. Phys. Condens. Matter* **2008**, *20*. [[CrossRef](#)]
29. Buschow, K.H.J.; van Engen, P.G. Magnetic and magneto-optical properties of Heusler alloys based on aluminum and gallium. *J. Mag. Mag. Mater.* **1981**, *25*, 90–96. [[CrossRef](#)]
30. Slebarski, A.; Goraus, J.; Deniszczyk, J.; Skoczen, L. Electronic structure, magnetic properties and electrical resistivity of the Fe<sub>2</sub>V<sub>1-x</sub>Ti<sub>x</sub>Al Heusler alloys: experiment and calculation. *J. Phys. Condens. Matter* **2006**, *18*, 10319–10334. [[CrossRef](#)] [[PubMed](#)]
31. Friák, M.; Hickel, T.; Körmann, F.; Udyansky, A.; Dick, A.; von Pezold, J.; Ma, D.; Kim, O.; Counts, W.A.; Šob, M.; Gebhardt, T.; Music, D.; Schneider, J.; Raabe, D.; Neugebauer, J. Determining the Elasticity of Materials Employing Quantum-mechanical Approaches: From the Electronic Ground State to the Limits of Materials Stability. *Steel Res. Int.* **2011**, *82*, 86–100. [[CrossRef](#)]
32. *Handbook of Chemistry and Physics*; CRC Press: Boca Raton, FL, USA, 1928.
33. Hohenberg, P.; Kohn, W. Inhomogeneous electron gas. *Phys. Rev. B* **1964**, *136*, B864–B871. [[CrossRef](#)]
34. Kohn, W.; Sham, L.J. Self-consistent equations including exchange and correlation effects. *Phys. Rev. A* **1965**, *140*, A1133–A1138. [[CrossRef](#)]
35. Kresse, G.; Hafner, J. Ab initio molecular dynamics for liquid metals. *Phys. Rev. B* **1993**, *47*, 558–561. [[CrossRef](#)]
36. Kresse, G.; Furthmüller, J. Efficient iterative schemes for ab initio total-energy calculations using a plane-wave basis set. *Phys. Rev. B* **1996**, *54*, 11169–11186. [[CrossRef](#)]
37. Blöchl, P.E. Projector augmented-wave method. *Phys. Rev. B* **1994**, *50*, 17953–17979. [[CrossRef](#)]
38. Kresse, G.; Joubert, D. From ultrasoft pseudopotentials to the projector augmented-wave method. *Phys. Rev. B* **1999**, *59*, 1758–1775. [[CrossRef](#)]
39. Perdew, J.P.; Wang, Y. Accurate and simple analytic representation of the electron-gas correlation energy. *Phys. Rev. B* **1992**, *45*, 13244–13249. [[CrossRef](#)]
40. Vosko, S.H.; Wilk, L.; Nusair, M. Accurate spin-dependent electron liquid correlation energies for local spin density calculations: a critical analysis. *Can. J. Phys.* **1980**, *58*, 1200. [[CrossRef](#)]
41. Williams, A.R.; Moruzzi, V.L.; Kübler, J.; Schwarz, K. *Bull. Am. Phys. Soc.* **1984**, *29*, 278.
42. Schwarz, K.; Mohn P. Itinerant metamagnetism in YCo<sub>2</sub>. *J. Phys. F* **1984**, *14*, L129–L134. [[CrossRef](#)]
43. Podgórný, M.; Thon, M.; Wagner, D. Electronic-structure and thermodynamic properties of Fe-Pt alloys. *J. Magn. Magn. Mater.* **1992**, *104*, 703–704. [[CrossRef](#)]
44. Singh, D.J.; Klein, B.M. Electronic-structure, lattice stability, and superconductivity of CrC. *Phys. Rev. B* **1992**, *46*, 14969–14974. [[CrossRef](#)]
45. Entel, P.; Hoffmann, E.; Mohn, P.; Schwarz, K.; Moruzzi, V.L. 1st-principles calculations of the instability leading to the invar effect. *Phys. Rev. B* **1993**, *47*, 8706–8720. [[CrossRef](#)]
46. Wu, S.Q.; Hou, Z.F.; Zhu, Z.Z. Elastic properties and electronic structures of CdCNi<sub>3</sub>: A comparative study with MgCNi<sub>3</sub>. *Solid State Sci.* **2009**, *11*, 251–258. [[CrossRef](#)]
47. Hsueh, H.; Crain, J.; Guo, G.; Chen, H.; Lee, C.; Chang, K.; Shih, H. Magnetism and mechanical stability of  $\alpha$ -iron. *Phys. Rev. B* **2002**, *66*. [[CrossRef](#)]
48. Fecher, G.H.; Chadov, S.; Felser, C. Theory of the Half-Metallic Heusler Compounds. In *Spintronics, From Materials to Devices*; Felser, C., Fecher, G.H., Eds.; Springer: Dordrecht/Heidelberg, Germany; New York, NY, USA; London, UK, 2013; pp. 115–166.
49. Brzakalik, K.; Frackowiak, J. A Mossbauer and structural study of disordered alloys Fe<sub>3-x</sub>Ti<sub>x</sub>Al (0 < x < 1). *Nukleonika* **2003**, *48*, S13–S16.
50. Yan, X.; Grytsiv, A.; Rogl, P.; Pomjakushin, V.; Palm, M. The Heusler Phase Ti<sub>25</sub>(Fe<sub>50-x</sub>Ni<sub>x</sub>)Al<sub>25</sub> (0 ≤ x ≤ 50); Structure and Constitution. *J. Phase Equilib. Diffus.* **2008**, *29*, 500–508. [[CrossRef](#)]

51. Momma, K.; Izumi, F. An integrated three-dimensional visualization system VESTA using wxWidgets. *Comm. Crystallogr. Comput. IUCr Newslett.* **2006**, *7*, 106. [[CrossRef](#)]
52. Momma, K.; Izumi, F. VESTA: a three-dimensional visualization system for electronic and structural analysis. *J. Appl. Crystallogr.* **2008**, *41*, 653–658. [[CrossRef](#)]
53. Momma, K.; Izumi, F. VESTA 3 for three-dimensional visualization of crystal, volumetric and morphology data. *J. Appl. Crystallogr.* **2011**, *44*, 1272–1276. [[CrossRef](#)]



© 2018 by the authors. Licensee MDPI, Basel, Switzerland. This article is an open access article distributed under the terms and conditions of the Creative Commons Attribution (CC BY) license (<http://creativecommons.org/licenses/by/4.0/>).